

See discussions, stats, and author profiles for this publication at: <https://www.researchgate.net/publication/263945872>

Nanoparticle Controlled Self-Assembly in Varying Chain Extended Polyurethanes as Potential Nanobiomaterials

ARTICLE in THE JOURNAL OF PHYSICAL CHEMISTRY C · JANUARY 2012

Impact Factor: 4.77 · DOI: 10.1021/jp210560s

CITATIONS

7

READS

11

5 AUTHORS, INCLUDING:



Biswa P. Das Purkayastha

Assam University

9 PUBLICATIONS 96 CITATIONS

[SEE PROFILE](#)



Vinod K Aswal

Bhabha Atomic Research Centre

392 PUBLICATIONS 4,906 CITATIONS

[SEE PROFILE](#)



Pralay Maiti

Indian Institute of Technology (Banaras Hin...)

102 PUBLICATIONS 3,641 CITATIONS

[SEE PROFILE](#)

Nanoparticle Controlled Self-Assembly in Varying Chain Extended Polyurethanes as Potential Nanobiomaterials

Abhinay Mishra,[†] Biswa Pratim Das Purkayastha,[‡] Jagat K. Roy,[‡] Vinod K. Aswal,[§] and Pralay Maiti^{†,*}

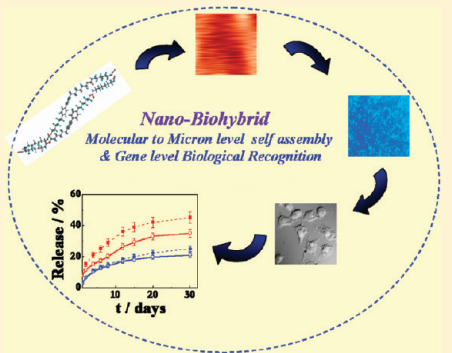
[†]School of Materials Science and Technology, Institute of Technology, Banaras Hindu University, Varanasi 221 005, India

[‡]Department of Zoology, Banaras Hindu University, Varanasi 221 005, India

[§]Solid State Physics Division, Bhabha Atomic Research Centre, Trombay, Mumbai 400 085, India

Supporting Information

ABSTRACT: Novel polyurethanes have been synthesized using aliphatic diisocyanate and aromatic chain extenders with varying spacer length. Nanohybrids of those polyurethanes have been prepared using two-dimensional surface modified nanoclay by dispersing it in poly-ol followed by prepolymerization and subsequent extension with chain extenders of a range of length scales. Dramatic improvement in toughness and adequate enhancement in stiffness in presence of nanoclay have been observed for higher spacer length of chain extender exhibiting no trade-off for these new classes of nanohybrids. Step-by-step self-assembly starting from nanometer dimension molecular association to micrometer scale crystallite has been revealed through electronic structure calculation, X-ray diffraction, small angle neutron scattering, atomic force microscopy, and optical images. The role of hydrogen bonding has been uncovered for this type of supramolecular assembly which further aggravated in presence of organically modified nanoclay by making bigger clusters for nanohybrids. The potential application for these nanohybrids as biomaterials has been verified through cell adhesion and cytotoxicity studies. Biocompatibility at the gene level was analyzed through the perspective of HIPK2, a member of the group involved in cell-cycle regulation. Sustained drug delivery has been testified by using bigger dimension of clusters formed by self-assembly. Another means of controlled drug delivery has been verified by dispersing disk-like two-dimensional nanoclay in polymer matrix by making diffusion barrier tortuous path.



INTRODUCTION

Self-assembly in polymers is being extensively revealed for tailoring and fabricating the structures in the nanoscale dimensions.^{1–5} Polymeric self-assembly has numerous advantages over conventional materials due to their explicit feature of assembling in highly ordered lamellar, spherical, and networked morphologies; as a matter of fact, these materials are having a superior thermo-mechanical property, which leads to metastable structure.^{6–11} In recent years, high performance self-assembled thermoplastic polyurethane have been extensively used in shape memory materials, molecular recognition, tissue engineering, and sustained drug delivery applications.^{12–15} The thermodynamic structural incongruity of hydrogen bonded hard and soft segmented domains in a regular fashion lead to unusual self-assembled patterning in thermoplastic polyurethanes.^{16,17}

The incorporation of nanoparticles as a potential reinforcing agent in the matrix of self-assembled polyurethanes produces the unparalleled combinations of strength, stiffness, and toughness in these novel nanohybrids.^{18–20} Wang and Pinnavaia were the foremost to observe the dramatic enhancement in the tensile strength and modulus by the incorporation of these 2-D nanoparticles in the thermoplastic polyurethane matrix.²¹ Subsequently, polyurethane nanohybrids have been explored due to interactions of 2-D nanoclay

tactoids with the alternating assembly of hard and soft segments. Moreover, the physicochemical and biological properties of polymeric self-assemblies can be tuned by varying chemical structure and the constituents present in the polymer backbone or by the presence of nanofillers.^{22–25} Nanofiller supported polymeric matrix may have the potential for cellular growth for tissue engineering. Recently, we have reported molecular level self-assembly starting from nanoscale organization to optically observable microscale crystallite for thermoplastics leading to patterned structures.²⁶ The tunability of self-assembled structure is still a challenge which might be realistic either by incorporating new chemical entity or by dispersing a second phase in the form of filler. The effect of modulated nanostructure and self-assembly has been unraveled for the unusual electronic, thermal, mechanical, barrier, and biological property enhancement.²⁷ The controlled cellular responses have been observed in the gene level through cell adhesion by monitoring the localization of HIPK2 protein inside the cell.²⁸ A number of kinases are activated as a reaction to DNA damage or genotoxic stress. A member of the serine/threonine kinase family, HIPK2, is activated and stabilized upon DNA damage and direct the cell toward p53-dependent apoptosis or

Received: August 19, 2011

Published: December 23, 2011

programmed cell-death.^{29,30} Upon activation and stabilization, HIPK2 is imported to the nucleus in the form of speckles and otherwise exported to the cytoplasm in an inactive form by High Mobility Group A1 (HMGAI) protein. This process causes the inhibition of the p53-dependent apoptosis.³¹ Hence, the nuclear localization of HIPK2 is an important determinant of its activity as pro-apoptotic activator, which has been very well documented.³²

In this work, the main goal is to design polyurethanes with varying hard segment length to study the effect of chain extension on the self-organization of the pristine thermoplastics as well as tuning the properties using 2-D surface modified inorganic nanoparticles. The presence of aliphatic spacer groups in the aromatic chain extended backbone has a deep implication on the assembly from molecular-level to micrometer order inducing drastic enhancement in the properties of thermoplastics with the help of 2-D inorganic nanoparticles. Moreover, these novel nanohybrids having superior properties are biocompatible and in this study, we resorted to the differential localization of HIPK2 for the study of the controlled cellular response of the pure polymers and their nanohybrids after the cells have sustained the naive chemical environment. Finally, the sustained release of ciprofloxacin hydrochloride drug is demonstrated by using a range of spacer length and nanoparticle by controlling the self-assembled cluster size.

■ EXPERIMENTAL SECTION

Materials. Poly(tetramethylene glycol) (PTMG) (terathane, Sigma-Aldrich; number average molecular weight (M_n) = 2900 g/mol), 1,6-hexamethylene diisocyanate (HDI) (Merck, Germany), Hydroquinone (HQ) and 4,4'-Biphenol (BP) (Sigma-Aldrich) were used as received. Organically modified nanoclay was methyl tallow bis-hydroxyethyl quaternary ammonium ion-exchanged montmorillonite (Southern clay, U.S., CEC 110 meq/100 g), (Cloisite 30B). The catalyst dibutyltin dilaurate and solvent dimethyl formamide (DMF) were purchased from Himedia and Merck, respectively. Ciprofloxacin hydrochloride was kindly gifted by Elcon Drugs and Formulation Ltd. Jaipur, India.

Synthesis of Chain Extender 4–4'-Bis(2-hydroxy ethyl) Biphenol (HEBP) and 4–4'-Bis (6-hydroxy hexyl) Biphenol (HHBP). HEBP was synthesized by refluxing BP and bromoethanol in slight basic medium in acetone. The reaction mixture was poured into water, filtered and the compound was purified by recrystallization from ethanol. In a similar way, HHBP was synthesized by refluxing BP and chlorohexanol in slight basic medium in ethanol. The reaction mixture was poured into water, filtered, and the compound was purified by recrystallization from 1-butanol.

Synthesis of Polyurethanes and its Nanohybrids. Synthesis of polyurethanes is considered to be a two step process. The first step generally refers to the formation of prepolymer using PTMG and HDI at 70 °C for 3 h to form an isocyanate-terminated prepolymer in a closed reaction vessel. The second step corresponds to the chain extension in which chain extenders (HQ, BP, HEBP or HHBP) have been added to prepolymer in presence of DMF as solvent and DBTDL as catalyst (0.1 ml of 1 wt.% toluene solution) to complete the polymerization reaction with rapid stirring at 70 °C for 24 h. The polymer was extracted by pouring the solution in deionized water (nonsolvent for PU) and dried under reduced pressure at 60 °C for 48 h. The hard segment content was kept constant (20%) by varying the molar ratios of PTMG: HDI: Chain Extender as shown in Supporting Information, SI, Table S1 for different chain extended polyurethanes.

Henceforth, the polyurethanes with different chain extenders HQ, BP, HEBP and HHBP will be designated as HQ-PU, BP-PU, HEBP-PU and HHBP-PU, respectively.

Nanohybrids were synthesized by incorporating 4 wt.% of 30B nanoclay at the first stage with molten PTMG followed by the addition of HDI to form nanoclay incorporated prepolymer mixture. Subsequently, chain extenders (HQ, BP, HEBP, or HHBP) in presence of DMF solvent and DBTDL catalyst (0.1 mL of 1 wt.% toluene solution) were added separately in the nanoclay incorporated prepolymer mixture with rapid stirring at 70 °C for 24 h. The nanohybrids were extracted by pouring the solution in deionized water and dried under reduced pressure at 60 °C for 48 h. The hard segment content was kept constant (20%) by varying the molar ratios of PTMG: HDI: Chain Extenders for different chain extended polyurethane nanohybrids as well and the molar ratios are presented in SI Table S1. The polyurethane nanohybrids thus formed with different chain extenders (HQ, BP, HEBP, or HHBP) will be designated as HQ-NC, BP-NC, HEBP-NC, and HHBP-NC, respectively. The average molecular weights and its distribution of pure PU as measured using gel permeation chromatography using DMF as eluent at 70 °C with 1 mL/min flow rate is ~32 000 the details are included in SI Table 1.

Structural Study. Bruker AXS D8 Advance wide-angle X-ray diffractometer with a graphite monochromator was used for performing X-ray diffraction using CuK α source with a wavelength of 0.154 nm. The generator was operated at 40 kV and 20 mA. The thin sheets of the samples, prepared by using compression molding technique, were placed on a glass sample holder at room temperature and were scanned at diffraction angle 2 θ from 1° to 40° at the scanning rate of 1° min⁻¹.

Small angle neutron scattering (SANS) experiments were performed on the spectrometer at the Dhruva reactor at Bhabha Atomic Research Centre, Mumbai, India. The data were collected in the scattering vector (q) range of $0.17 \text{ nm}^{-1} \leq q \leq 3.5 \text{ nm}^{-1}$. The scattering from the samples were corrected for background contribution. The lower q range was fitted separately with Ornstein-Zernike and other models. The characteristics length (Λ_c) was calculated using the equation $\Lambda_c = 2\pi/q_m$, where q_m is the scattering vector q corresponding to the peak position of the shoulder in the scattering pattern. The temperature was kept constant at 30 °C during every measurement.

The UV-vis measurements have been carried out by using Shimadzu (UV-1700), Pharma Speck, UV-vis spectrophotometer operating in the spectral range of 200–1100 nm using thin solid film and drug loaded polymer film for release study. Infrared spectra were recorded on a Thermo Nicolet 5700 FTIR of thin solid polymer film taking 100 scans with the resolution of 4 cm⁻¹.

Thermal Behavior. The degree of crystallinity, melting, crystallization temperatures, and heats of fusion of the pure PU and its nanohybrids were determined by using Mettler 832 differential scanning calorimeter (DSC) over a temperature range of -100 to 200 °C at a scan rate of 10 °C min⁻¹. The peak temperature and enthalpy of fusion for first run were measured from the endotherms using a computer attached with the instrument. After the first melting, the samples were quenched at 100 °C min⁻¹. The peak temperature and enthalpy of fusion for the second run were also measured. The DSC was calibrated with indium before use.

Morphological Investigation. The morphology of pure PUs and their nanohybrids was investigated by using scanning electron microscope (SEM), atomic force microscope (AFM),

and polarizing optical microscope (POM). The nanoclay dispersion in the matrix was checked by using TEM (Technai G²) operated at an accelerating voltage of 100 kV. A thin layer, around 70-nm thick, from the nanohybrid sample was sectioned at -80.0 °C using a Leica ultramicrotome equipped with a sharp glass knife. The surface morphology of polyurethane and nano-hybrid flakes were examined with a Hitachi H-7100 scanning electron microscope operated at an accelerating voltage of 10 kV. All of the samples were gold-coated by means of a sputtering apparatus under vacuum before observation. Atomic force microscopy was performed using an NT-MDT multimode AFM, Russia, controlled by a Solver scanning probe microscope controller. Tapping mode was used with the tip mounted on 100 μm long, single beam cantilever with resonant frequency in the range of 240–255 kHz, and the corresponding spring constant of 11.5 N/m. Bulk morphology of thin film (~30 μm) in optical range was examined using a polarizing optical microscope (POM) (Leitz) after quenching the samples at room temperature on a Mettler hot stage.

Mechanical Properties. For tensile testing, standardized specimens were prepared via microinjection using microinjector (model FD-1, Fly Tech Engineering). The samples were micro-injected at a barrel temperature of $T_m + 20$ °C and mold temperature of 25 °C with a pressure of 100 bar. Tensile tests were performed with the injection-molded samples using an Instron 3369 tensile tester at a strain rate of 5 mm/min at room temperature with specimen dimension of 25 mm gauge length, 4.05 mm breadth and 2.12 mm thickness. Several samples were tested to obtain good error estimates.

Cell Adhesion and Genotoxicity. Epithelial cells, SiHa, was used and the methodology employed in this study has been discussed in an earlier report.²⁶ SiHa cells were cultured on glass substrate for 24 h in DMEM supplemented with 10% heat-inactivated FCS (GIBKO) and antibiotics in a humidified 5% CO₂ incubator at 37 °C. The cells were washed with 1X PBS and then treated with cisplatin (Fresenius Kabi Oncology Ltd., India) at concentrations of 3, 4, 5, and 6 μg mL⁻¹ in a fresh media for 24 h to generate genotoxic stress in the cells. The cells were then washed two times with 1X PBS and fixation was done in 4% PFA for 10 min. The fixed cells in the coverslip were washed and permeabilized with 0.1% PBST (1XPBS + 0.1% Triton X-100) for 10 min each and subsequently blocked with blocking solution (1X PBS, 0.1% sodium deoxycholate, 0.1% Triton-X, 0.1% BSA, 10% Fetal Calf Serum, 0.02% Thiomersal) at room temperature for 2 h. Primary antibody (Goat anti-HIPK2, Santa Cruz Biotech. Inc. at the dilution of 1:200) incubation was for overnight at 4 °C and was washed twice for 10 min with 0.1% PBST. Precleared secondary antibody (Donkey anti-goat Cy3, Molecular Probes at the dilution of 1:200) was incubated for 2 h at room temperature. The cells were again washed for 10 min twice with 0.1% PBST followed by counterstaining with DAPI (4'-6-diamidino-2-phenylidone dihydrochloride, Sigma, U.S.) was done for 15 min. A single wash with 0.1% PBST was done and finally slides were mounted with DABCO (antifading agent). For estimation of the percentage of cells showing nuclear or cytoplasmic localization of the protein, Nikon E800 microscope was used and optical image was collected from confocal microscope (Zeiss: LSM 510Meta). The images were modified in Adobe Photoshop. Thin film of polymer and its nanocomposites were coated onto glass substrate to check whether the polymers are toxic for the cells. The polymer and composites coated glass were then sterilized by using UV irradiation for 2 h and then cells were seeded onto them along with control (5 μg mL⁻¹ of cisplatin). The cells were then processed as above.

Drug Assay and Release Study. Ciprofloxacin hydrochloride standard stock solution (1 mg/mL) was prepared first. Standard curve was drawn after taking absorbance using UV-vis spectrophotometer (Shimadzu 1700) at 277 nm in the concentration range 1–10 μg/mL (SI Figure S1). The in vitro release study was performed in PBS buffer at pH ≈ 7.4. Drug embedded pristine polyurethanes and its nanohybrids, prepared using solution route followed by evaporation of solvent, were put in 100 mL of release medium at incubator shaker at 100 rpm at 37 °C. Samples were withdrawn from the release medium at a particular time intervals and similar quantity was replaced with fresh buffer. The concentration of antibiotic drug in the sample was measured by taking absorbance at 277 nm.

RESULTS AND DISCUSSION

Wide Variation in Nanostructure. The effect of chain extenders on the dispersion of nanoclay in the polyurethane matrix has been presented in Figure 1a. The (001) peak of nanoclay ($d_{001} = 1.8$ nm; $2\theta \approx 4.8^\circ$) has been shifted toward lower angle in HHBP-NC and the corresponding d -spacing of organically modified nanoclay increases to 3.7 nm ($2\theta \approx 2.38^\circ$) due to intercalation of polymer chains while the absence of any peak in HQ-NC, BP-NC, and HEBP-NC indicates exfoliated/disordered structure. Interestingly, two crucial factors dictate the ultimate nanostructures; number of aromatic rings and the length of spacer group attached to these aromatic rings in the chain extenders that form the long chain polymer. The effect of spacer group length gradually increases from BP to HHBP (Scheme I). In all cases, the polymerization occurs inside the gallery of the nanoclays. The proximity of formation of intermolecular hydrogen bonding (between urethane linkages) increases with the spacer length in the chain extenders due to stereochemical orientation of the biphenyl/benzene ring. The typical molecular aspect behind the intercalation phenomenon appears when the hydrogen bonded interaction between two polymer chains exceeds the van der Waals interaction between the polymer moiety and nanoclay tactoids. The effective interaction through hydrogen bonds increases as the interaction site is away from the π -clouds of the biphenyl ring as evident from the appearance of prominent hydrogen bonded N–H peaks at ~3320 cm⁻¹ against the disappearance of free N–H stretching frequency at 3500 cm⁻¹ in nanohybrids (Figure 1b) and will be discussed in detail in the simulation section. However, lesser intermolecular hydrogen bond and stronger interaction between organically modified nanoclay and polar polymer chain favor enhanced intercalation peak leading to exfoliation in HQ-NC, BP-NC, and HEBP-NC systems. So, the spacer length controls the intercalation and nanostructure greatly varies on the chain extender used for polymerization. It is quite obvious that nanostructures are absent in HQ-PU, BP-PU, and HEBP-PU while a small peak at $2\theta \approx 3.8^\circ$ appears for HHBP-PU corresponding to the distance between molecular planes ~2.3 nm, presumably due to extensive hydrogen bonding as mentioned before (SI Figure S2). In order to make a better understanding, we have investigated the nanostructures for higher hard segment content specimens e.g., ~70% HSC showing distinct peak in the same position (SI Figure S3) and a hump in lower spacer length of BP-PU. The extent of hydrogen bonds is prominent in case of higher HSC polymer showing better coherency in XRD pattern due to stronger aggregation linked through hydrogen bonding. The representative dispersion of nanoclay in PU matrix has been shown in Figure 1c indicating intercalated pattern of the nanohybrid.

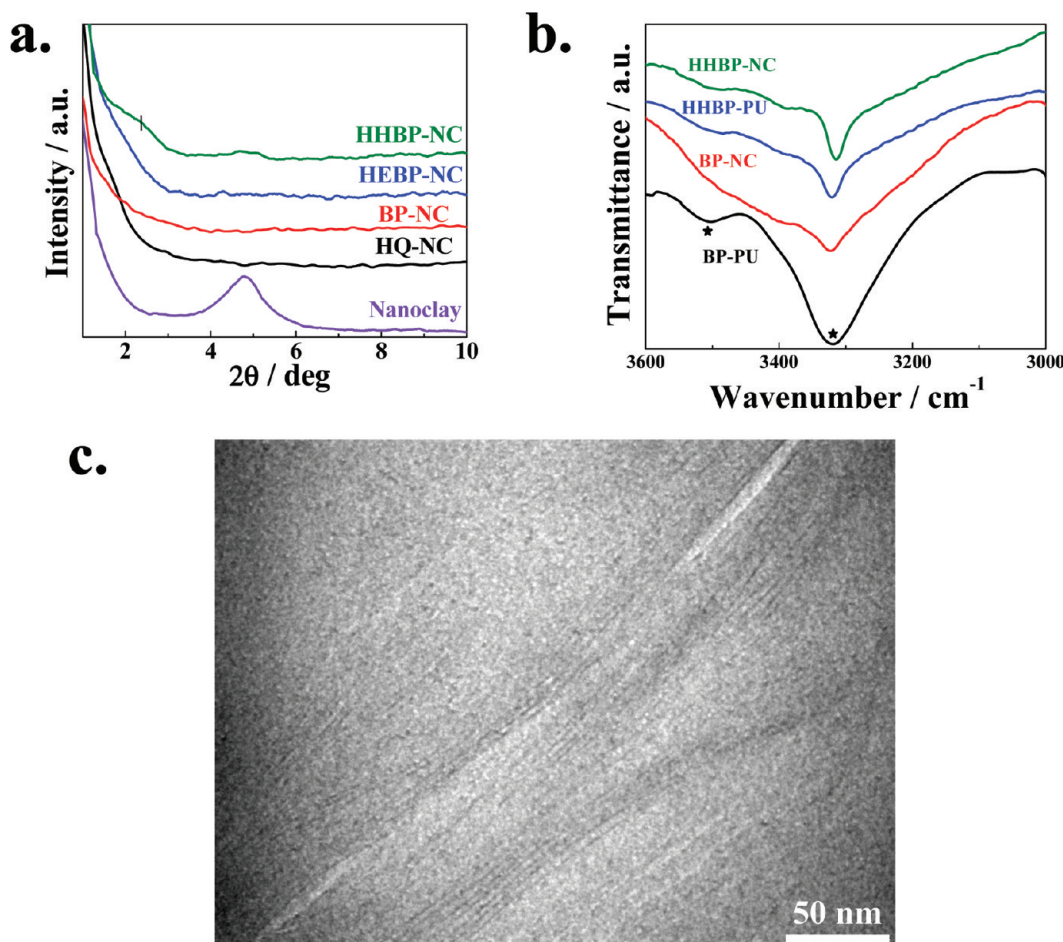
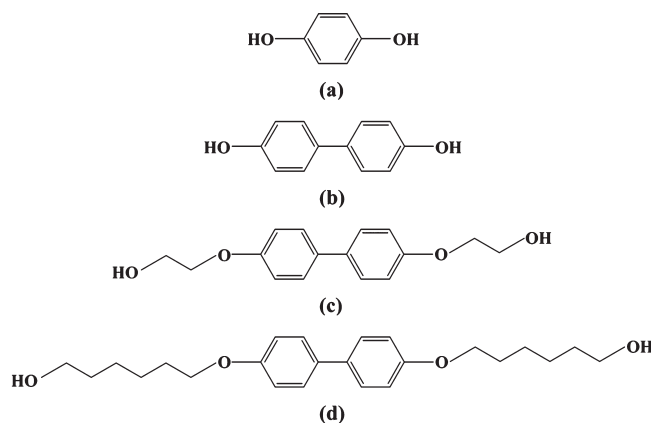


Figure 1. (a) Wide-angle X-ray diffraction of organically modified nanoclay and aromatic chain extended PU nanohybrids. (b) FTIR patterns of indicated pure polyurethanes and their nanohybrid. * marks indicate the free and hydrogen bonded N—H stretching peaks. (c) Bright field transmission electron micrograph of HHBP-NC nanohybrid.

Scheme 1. Chemical Structure of Different Chain Extenders Used and Their Designation (a) Hydroquinone (HQ), (b) 4,4'-Biphenol (BP), (c) 4,4'-Bis(hydroxyethyl) Biphenol (HEBP), and (d) 4,4'-Bis(hydroxyhexyl biphenol) (HHBP)



Tuning of Structure and Morphology. The variation of crystallinity of pure polymer and its nanohybrids strongly depends on the type of chain extenders and/or spacer length used for polymerization. Pure HQ-PU is amorphous while

crystallinity gradually develops with increasing spacer length as indicated by the presence of increasing crystalline peaks (at $\sim 19.8^\circ$ and 24.2° corresponding to 200 and 210 planes, respectively).³³ (Figure 2a) and the corresponding nanohybrids show greater crystallinity vis-à-vis pure polymers (Figure 2b). Higher crystallinity has also been confirmed through polarizing optical images of pristine polymer and their nanohybrids (Figure 2c). The microdomains gradually increase with higher spacer length PU and all of the subsequent nanohybrids illustrate larger and higher number density of crystallites. Differential calorimetric studies also confirm the higher crystallinity of nanohybrids and PU with higher spacer length as evident from the respective heat of fusion values (Figure 2d). Slight crystallinity develops in HQ-NC against complete amorphous nature for HQ-PU, while HEBP-PU and HEBP-NC are crystalline with the heat of fusion (ΔH) of 18 and 45 $\text{J}\cdot\text{g}^{-1}$, respectively. Simultaneously, the endothermic peaks for HQ-NC, BP-NC, HEBP-PU, HEBP-NC, HHBP-PU, and HHBP-NC appear at 142, 156, 150, 161, 154, and 162 $^\circ\text{C}$, respectively, indicating thicker and ordered crystallites in nanohybrids as compared to respective pure polymer. This is to mention that HQ-PU and BP-PU emerge as amorphous materials. The 2D-nanoparticle induced crystallization is discernible in nanohybrids and at the same time crystalline domain size increases as compared to pristine polymer as evident by XRD, POM, and DSC studies.

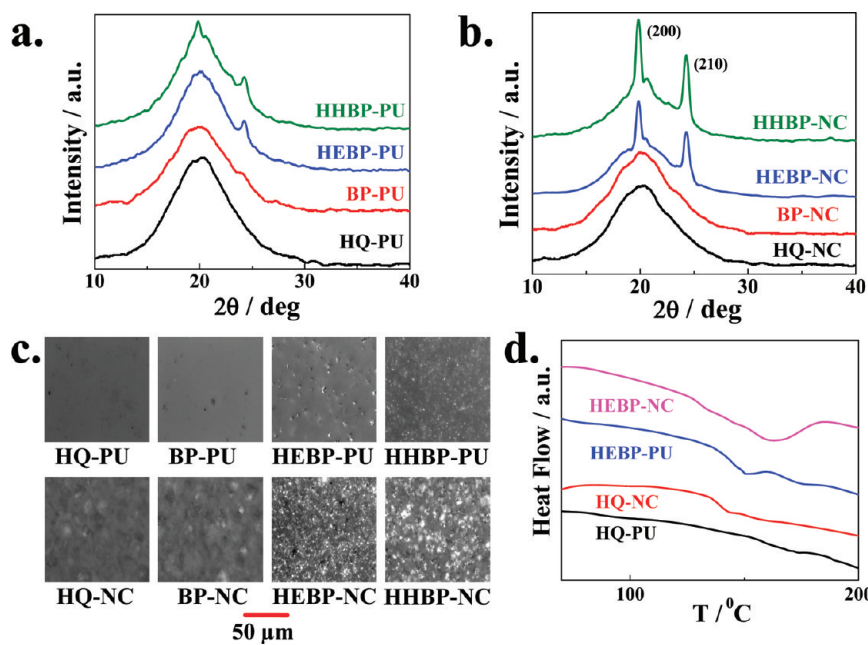


Figure 2. (a) XRD patterns of aromatic chain extended indicated pure PU. (b) XRD patterns of aromatic chain extended PU nanohybrids. (c) Polarizing optical images of aromatic chain extended PU and its nanohybrids. (d) DSC thermograms of aromatic chain extended PU and its nanohybrids in the first run. The Y-axes have been shifted for better clarity.

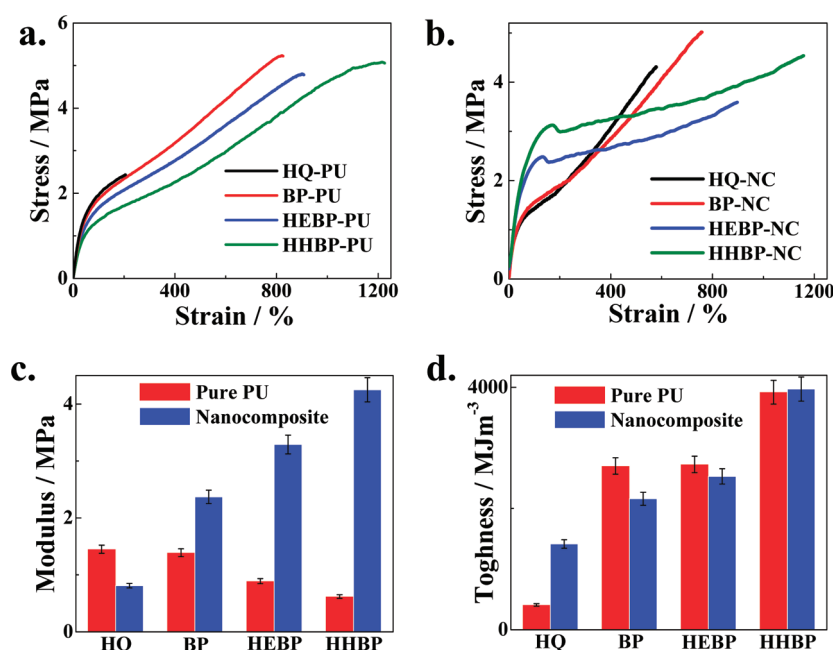


Figure 3. Mechanical responses of aromatic chain extended pure PU and its nanohybrids. (a) Stress-strain curves of indicated pure PU. (b) Stress-strain curves of respective nanohybrids. (c) Comparison of modulus values of pure PU and respective nanohybrids as indicated in the bar graph. (d) Comparison of toughness values of PU and its nanohybrids as indicated in the bar graph.

Moreover, the similar development of crystallinity occurs with increasing the spacer length of chain extender. The incorporation of nanoparticles cannot induce crystallinity when only aliphatic low spacer length (4-carbon chain) diol was used as a chain extender,²⁶ while in this study biphenyl and longer spacer with biphenyl/chain extended biphenyl ring facilitate the hydrogen bond formation, thereby, assist inducing crystallinity in PU. However, crystallinity can be tuned in pristine polymer as well

as in the nanohybrids especially with the extended spacer of chain extenders.

Mechanical Responses. The outcome of the structure and morphology has been verified through mechanical properties of pure polymers and their nanohybrids. The stress-strain behavior of pure PUs has been presented in Figure 3a showing significant and systematic increase of elongation at break with increasing spacer length. Further, there is considerable increase

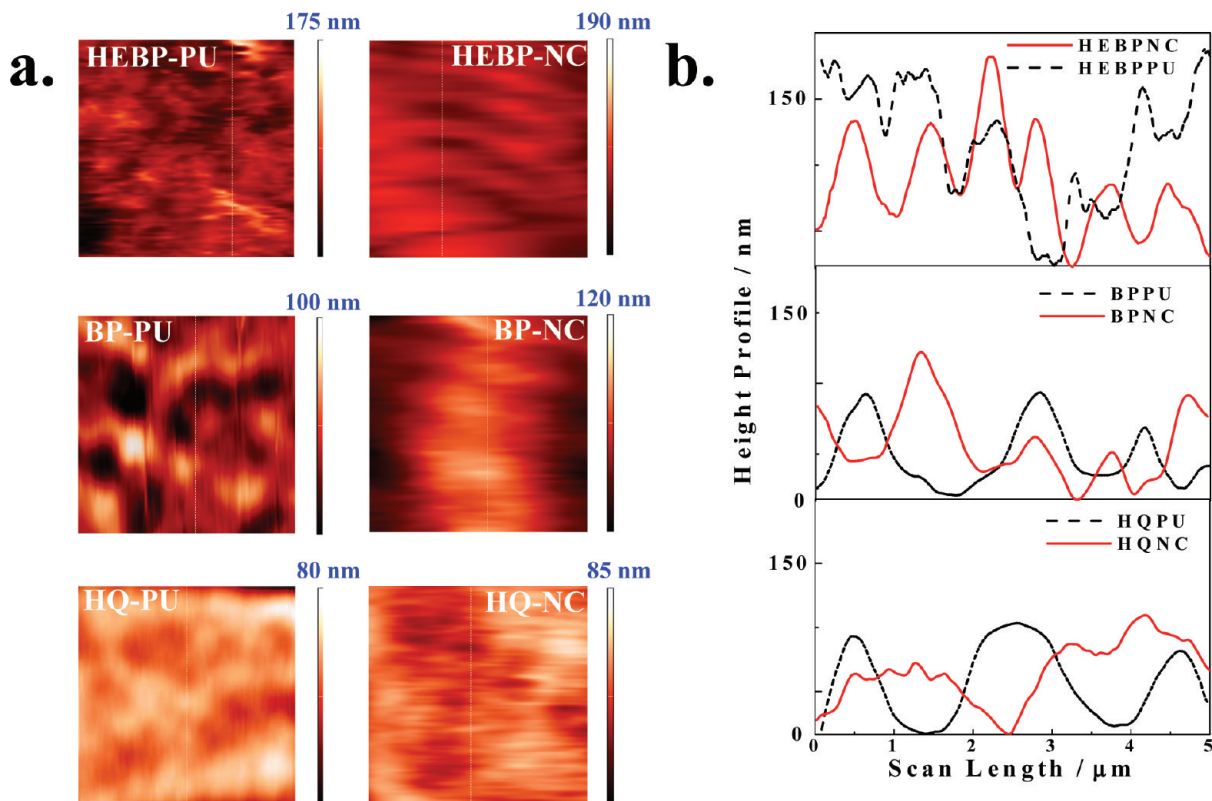


Figure 4. (a) AFM images of indicated aromatic chain extended PU and its nanohybrids ($5 \times 5 \mu\text{m}$) obtained through tapping mode. (b) AFM height profile patterns for $5 \mu\text{m}$ scan length as shown by the dotted lines in (a) of aromatic chain extended PU and its nanohybrids.

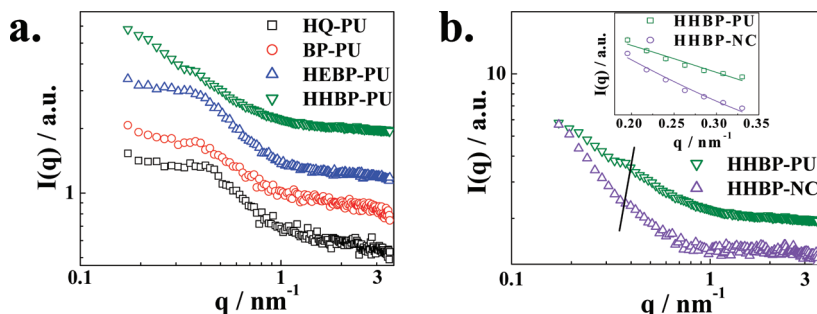


Figure 5. (a) Small-angle neutron scattering patterns; $I(q)$ vs q (wavevector) plot of indicated aromatic chain extended pure PU. (b) Small-angle neutron scattering patterns; $I(q)$ vs q (wavevector) plot of indicated PU and its nanohybrid. Inset figure shows the show the Ornstein-Zerlike fitting for the calculation of correlation length, ξ .

in elongation at break for HQ-NC nanohybrid (Figure 3b) as compared to pristine HQ-PU, where breaking strain was meager. The Young's modulus, as measured from the linear elastic regime, indicates steady decrease of tensile modulus with increasing spacer length and noteworthy improvement of modulus in respective nanohybrids (Figure 3c). Moreover, the toughness as measured from the area under stress-strain curves illustrates higher or comparable toughness for nanohybrids showing no trade-off after the hybrid formation (Figure 3d), usually observed for most polymer composites. The elastomeric nature of pure PUs (without any yield point) show strong strain induced hardening for short spacer length chain extender while typical thermoplastic behavior (with well-defined yield point) for longer spacer length chain extender and in nanohybrids is noticed

indicating stiffer materials induced by longer spacer of hard segment and 2-D nanoparticle in HEBP-NC and HHBP-NC systems. The paradigm improvement in mechanical response as a function of spacer length generally depends on the shape, size and concentration of the hard domains, intermolecular bonding within the hard domains and the ability of soft segment to crystallize under strain.^{34–36} In this study at constant hard segment content, the length of the chain extender present within the hard segment tunes the modulus and the toughness of the polyurethane. The presence of phenyl ring and aliphatic spacer length in general is responsible for high mechanical strength of the pristine polyurethanes. The cohesion of the hard segments and intermolecular hydrogen bonding within the domains results in the higher value of elongation at break for HHBP-PU as

compared to that of HQ-PU and BP-PU. Subsequently, the elongation at break for nanohybrid of HHBP system, i.e., HHBP-NC is also higher than that of HQ-NC and BP-NC. Strain induced crystallization is becoming prominent with the coherency of chain extended phenyl groups attached along with spacer group as well as with the few percent of incorporated nanoclay tactoids (Figure 3b). Toughness as measured from the area under stress-strain curves dramatically increases for HHBP-PU, HHBP-NC as compared to that of the HQ-PU, HQ-NC system. The reason lies behind the structure of the HHBP-PU where spacer attached biphenyl ring helps suppressing the crack propagation by orienting toward the applied force field while in the case of HHBP-NC orientation of individual clay tactoid is also an additional factor for enhanced toughness as compared to lower spacer length PU (Figure 3d). In contrast, 5-fold increases in modulus has been recorded for HHBP-NC as compared to respective pure polymer primarily because of intercalation (sandwich effect) and flocculation of nanoclay which enhances the ultimate aspect ratio of pure nanoclay. An increasing trend of enhancement in modulus from HQ-NC to HHBP-NC has been observed in nanocomposites while it decreases from HQ-PU to HHBP-PU. The meager improvement in toughness of absolute 170 MJ/m^3 value¹⁸ (15% higher as compared to pure PU) and up to 500% of elongation²⁰ are reported in the literature in presence of laponite clay and the superiority of this study (improvement up to 4000 MJ/m^3 toughness and 1200% elongation) lie on the in situ preparation of nanohybrids and designing of better chain extenders ensuing greater interaction and property improvement. However, one can tune the stiffness, strength and toughness of polyurethane by designing suitable polyurethane and nanocomposites using different chain extenders and inorganic filler combination.

Nanoparticle Induced Self-Assembly. The domain structure in microscale was evident in pure polyurethane which becomes prominent and organized in the case of nanohybrids especially for HEBP-NC and HHBP-NC (Figure 2c) under crossed nicol optical microscope. More ordered cylindrical domains, within the above domain in optical micrographs, have been observed in AFM topographs in tapping-mode for all the pure PUs and nanohybrids (Figure 4a). Figure 4b shows the height profile assessment of pure PUs and nanohybrids showing gradual increase of height sketch with increasing spacer length which further increase in presence of nanoclay in nanohybrids in all the cases indicating compact and dense crystallite in presence of nanoclay and with increasing spacer length. The average roughness values of the entire micrograph are 85, 96, 130, 136, 188, and 196 nm for HQ-PU, HQ-NC, BP-PU, BP-NC, HEBP-PU, and HEBP-NC, respectively. The contrasts appear in AFM images presumably because of segmented microcrystalline zones in polymer films and the surface roughness profile of the nanohybrids is higher vis-à-vis pure polymer (80–200 nm) as discernible in Figure 4b signifying nanoclay induced clustering/self-assembly. Moreover, the development of the small angle neutron scattering (SANS) peaks at $q \approx 0.4 \text{ nm}^{-1}$, corresponding to the characteristic length, $\Lambda_c = 2\pi/q_m \approx 15–18 \text{ nm}$ indicates a nanostructure (Figure 5a) within the microdomains as observed in AFM topographs. The lower value of Λ_c for HHBP-PU ($\sim 15 \text{ nm}$) as compared to HQ-PU ($\sim 18 \text{ nm}$) indicates that the lesser number of molecular sheets are required to form an assembly as the phenyl rings attached with longer spacer groups increase the proximity of hydrogen bonded interaction sites due to preferred stereo conformations. The similar rationale applies

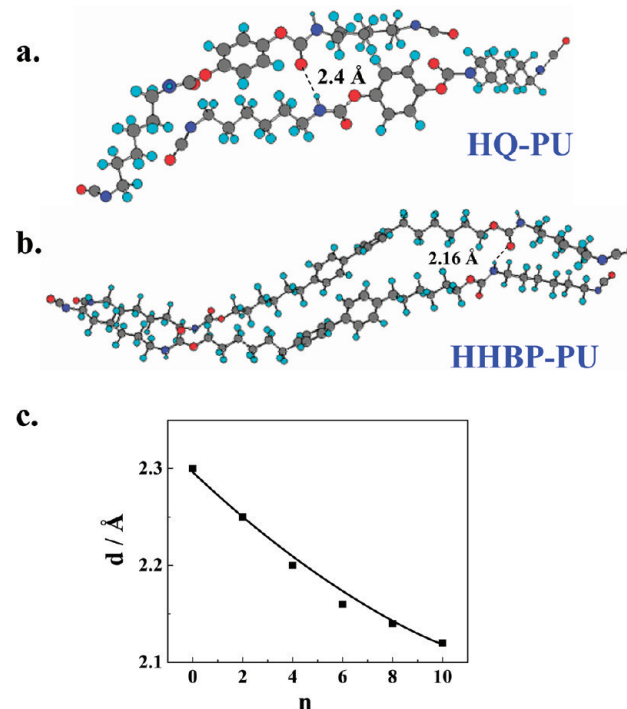


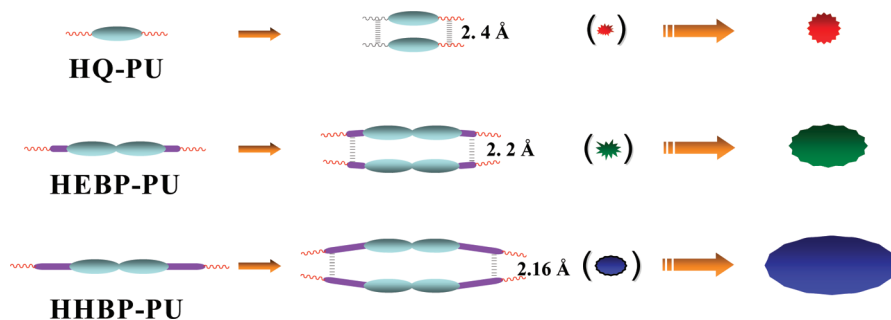
Figure 6. Molecular models of aromatic chain extended polyurethane obtained from energy minimized electronic structure calculation from a part of chains showing the distance of hydrogen bonded interaction sites leading to self-assembly for (a) HQ-PU and (b) HHBP-PU, and (c) Hydrogen bonded inter chain distances as a function of aliphatic alkyl spacer group length attached to aromatic biphenyl chain extender.

for the lower Λ_c value for HHBP-NC ($\sim 16 \text{ nm}$) as compared to HQ-NC ($\sim 22 \text{ nm}$) in presence of 2-D nanoclays which further facilitate the self-assembly in nanohybrids (Figure 5b). The characteristic length ($\Lambda_c = 2\pi/q_m$, where q_m is the wavevector at peak maxima) gradually decreases as 18, 17, 16, and 15 nm for pure HQ-PU, BP-PU, HEBP-PU, and HHBP-PU, respectively, indicating the close packed lamellar distribution with introduction of phenyl rings and/or longer spacer groups. The nanohybrids exhibit the similar fashion (Λ_c s are 22, 21, 18, and 16 nm for HQ-NC, BP-NC, HEBP-NC, and HHBP-NC, respectively) but the absolute values are somehow higher side vis-à-vis pristine polymer presumably due to insertion of nanoclay in the hard segment zone resulting from dipolar interaction and follow the exact trend of interaction (high in HQ system and low for HHBP system) as observed in nanostructure. The SANS patterns are best fitted with Ornstein-Zernike model (eq 1);

$$I(q) = \frac{I(0)}{1 + \xi^2 q^2} \quad (1)$$

where, $I(q)$ is the scattered intensity, $I(0)$ is the extrapolated structure factor at zero wavevector and q is wavevector, providing the correlation length, ξ in the range of 1 - 4.5 nm for pure PUs and 3 to 5.5 nm for nanohybrids (inset of Figure 5b and SI Figure S4). The ξ values are 1, 1.5, 3, and 4.5 nm for pure HQ-PU, BP-PU, HEBP-PU, and HHBP-PU, while they are 3, 3.5, 4.8, and 5.5 nm for HQ-NC, BP-NC, HEBP-NC, and HHBP-NC, respectively. The ξ value essentially represents the size of blob which increases with spacer length and with the incorporation of nanoclay in respective PUs. Hence, the SANS data designate the

Scheme 2. Schematics Showing the Bottom up Approach Starting from the Molecular Level to the Micrometer Level Cluster Formation^a



^a Starting from the single chain of HHBP-PU assembles in a regular fashion to form extensively hydrogen bonded network which accumulates to generate polymer domains/clusters as noticed in SANS and AFM studies. These polymer domains/clusters further accumulates to micro-scale crystalline domain as observed in POM. Spacer group attached with aromatic chain extender is solely responsible for the extensive hydrogen bonded microcrystallites. The interchain distance is smallest in the case of HHBP-PU, while it increases for HEBP-PU and BP-PU gradually.

lamellar organization within the microcrystallite and quantitatively measure the blob size depending on the spacer length and insertion of nanoclay.

In order to understand the role of phenyl, biphenyl, and biphenyl rings with variant aliphatic spacer groups on the assembly of polyurethanes, the conformation of molecules in its energy minimized state have been construed by using semiempirical AM1 method (electronic structure calculations). The lowest energy conformation of HQ-PU based aromatic polyurethane chain with the shortest hydrogen bonded distance between C=O and H–N intermolecular group is 2.4 Å (Figure 6a). However, the lowest energy of HHBP-PU took a loop-like shape with the minimum distance between the above pair approaches to 2.16 Å (Figure 6b). However, a close loop conformation has been anticipated due to preferred orientation of C=O and H–N group for HHBP-PU, to constitute a molecular sheet/plane through H-bonding, which is the basis for constructing the nanostructure. On the contrary, the minimum distance between two molecules in the case of the HQ-PU is 2.4 Å and π stacking of aromatic rings is not sufficient to construct an ordered molecular plane. Moreover, the minimum intermolecular distance of PUs gradually decreases from 2.4–2.16 Å as a function of spacer length attached to biphenyl group (Figure 6c) indicating stronger hydrogen bonded interactions between C=O and H–N group for larger aliphatic group spacer length (discussed in the FTIR section). Nonetheless, the planar molecular structure is evident for HHBP-PU, whereas HQ-PU has non planar structure due to poor H-bonding in the vicinity of the phenyl ring primarily due to steric reason which is categorically less for larger spacer PUs as the hydrogen bonding occurs away from the π -stacking of the biphenyl ring. The higher the spacer length stronger is the hydrogen bond formation. Now, the bottom-up approach is evident where molecular planes, as observed through molecular modeling, stacked in a regular fashion through extensive hydrogen bonding to form stacks of molecular layered sheet structures, revealed by SANS and XRD peak, assembled to form a domain, observed in AFM, which further accumulated into microclusters as discernible in crystallites using POM resulting to the systematic assembly starting from nanostructure to microstructure. The step-by-step self-assembly has been shown in Scheme 2, where the intermolecular hydrogen bonded distance varies with spacer length as calculated through electronic structure optimization. Subsequently, few of

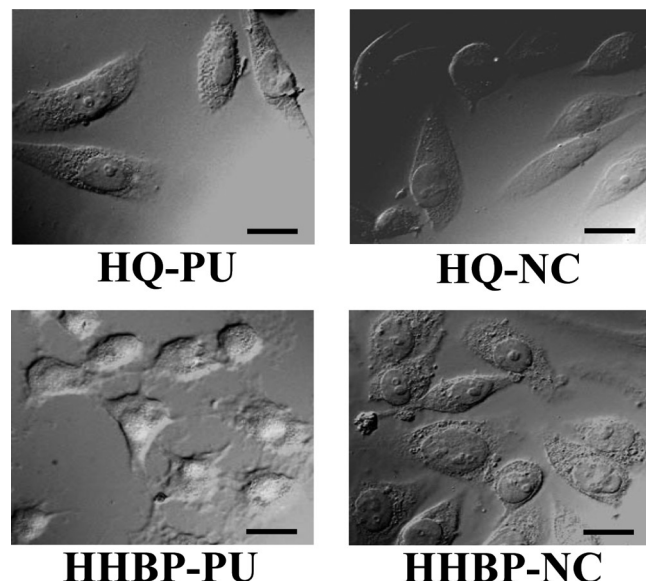


Figure 7. DIC images of cells grown on indicated PU and its nano-hybrids. Cells are in a quite healthy condition after adherence ($t = 48$ h) on to the surface of HQ-PU, HQ-NC, HHBP-PU, and HHBP-NC. (Scale bar = 10 μ m).

those hydrogen bonded molecule stack together to form sheet-like structure which is realized from the Bragg's reflection in SANS pattern ($d \approx 15\text{--}22$ nm). Again some of the sheet-like geometries put together and appear in band-like morphology (size $\sim 200\text{--}500$ nm) observed in AFM images.^{26,27,37} Finally, band-like assembly further accumulate to form bigger crystallite (micrometer size) observe in optical images. The primary reason for all these assemblies is extensive hydrogen bonding which gets facilitated in presence of nanoclay, due to presence of hydroxy-ethyl group in the organic modifier and edge hydroxyl group of nanoclay, exhibiting larger assembly in nano-hybrids vis-à-vis pristine PUs.

Biological Recognition and Genotoxicity. Integration of the nanoparticles with the polymer of varying self-assembled patterns alters the physical and chemical properties of the polymer. The responses of the biological system to such alteration with improved mechanical and self-assembled properties have been studied through a two-step approach, for the discernment of the

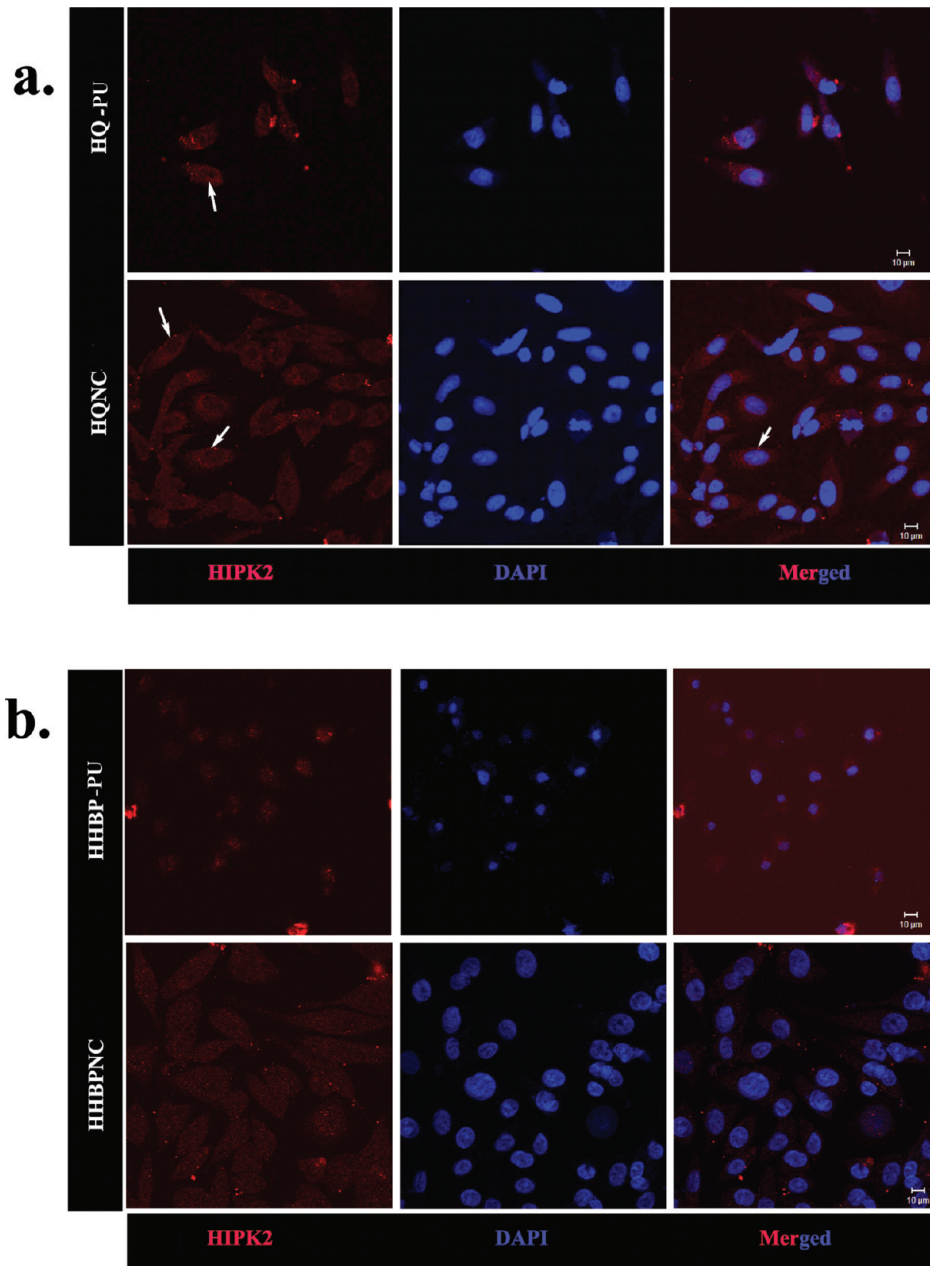


Figure 8. Confocal Laser Scanning micrographs of (a) HQ-PU and HQ-NC (b) HHBP-PU and its nanohybrid HHBP-NC. The panel shows the localization of the pro-apoptotic activator, HIPK2, in the cells and appeared to be similar in all the categories. DAPI (4'-6-diamidino-2-phenylidone dihydrochloride), was used to counter stain the nucleus. (Scale bar = 10 μ m).

biocompatibility^{38–42} of the nanohybrids. The first step helps decipher if the pure polymer and its nanohybrids provide the ambient environment for the adhesion and growth of adherent epithelial cells or not. The next step enhances the knowledge further, where the biological health of the cells growing over the pure polymer or its nanohybrids was verified with the help of a cellular marker. Adherent cells are indicative of their status of being alive. Trypsinized cells were seeded on thin polymer films (pure and nanohybrids) coated onto glass substrates. The epithelial cells appeared to be well-adapted to HQ-PU and its nanohybrids as the cells retained their structural integrity (Figure 7) and the result was reproducible. The adaptation was confirmed by studying the localization of the cellular marker,

HIPK2, in such cells. The nucleus was almost devoid of any HIPK2 speckles (indicated by white arrow in Figure 8a) in cells grown over HQ-PU and its nanohybrid, HQ-NC. In this experiment, cisplatin was used as a positive control for inducing genotoxic stress inside the cells, resulting in the activation of HIPK2, whereby it is imported to the nucleus of the cell in speckles. The standardization of the dose of cisplatin and its application in the form of usage of HIPK2 as a marker has been discussed earlier.²⁶ The staining pattern observed in pure HQ-PU and HQ-NC was similar to the untreated one (0 μ g/mL) (SI Figures S5 and S6). HIPK2 in those cells do not appear to be apparently getting activated, which is indicative of the fact that pure HQ-PU and its nanohybrid do not elicit any negative response

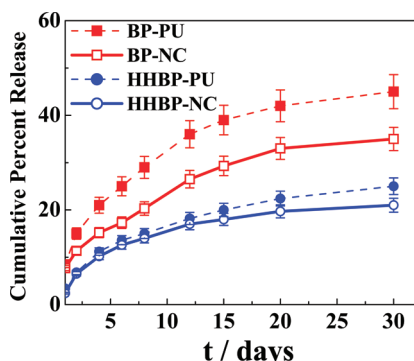


Figure 9. Sustained drug release profile of indicated PU and respective nanohybrids.

from the growing cells. Nevertheless, the facet of the result deviated, when observed in HHBP-PU and its nanohybrid, HHBP-NC. In pure HHBP-PU, the cells presented an abnormal structure, which can be visualized in the photomicrographs obtained from bright field microscope (Figure 7). Although the cells were reduced in overall size and carried a deformed look, they remained adhered to the surface of the HHBP-PU. It appeared that the pure polymer is imparting a negative influence on the cells, which was also evident from the strong nuclear localization of HIPK2 in such cells (Figure 8b). The structural identity of the cells grown on HHBP-NC in terms of size and shape (Figure 7) were comparable to the normal cells. Factually, it can be stated that the structural characteristic of the cells were restored when grown on its nanohybrid (HHBP-NC). This was confirmed by immunostaining of HIPK2, where bulk of HIPK2 was cytoplasmically localized. Little or no nuclear localization of the protein could be observed. This hints at the fact that the nanohybrid (HHBP-NC) is more compatible biologically as compared to pure HHBP-PU. The reason of more biocompatibility of nanohybrids lie on more hydrophilic nature of NC as compared to pure polymer as evident from the lower contact angle of HHBP-NC ($66 \pm 1^\circ$) than that of pure HHBP-PU ($73 \pm 1^\circ$).⁴³ The improvement in cell viability, measured through cell counting and growth behavior, in CNT-filled poly(lactide-co-caprolactone)⁴⁴ and chitosan-MMT composite⁴⁵ as compared to respective pure copolymer/polymer suggests filled system might be a better biocompatible system than that of pristine matrix either due to surface roughness or hydrophilic nature. Hence, the study emphasizes the fact that mere survival of cells in the polymer environment might turn out deceptive of the cellular health and nanoparticles exert a conducive environment for the proliferation and growth of the cells. Nanohybrids are mechanically and thermally superior, along with a better medium for cellular growth and, hence, suitable for scaffold materials with stiffer and tougher by design.

Sustained Drug Release. In the previous section, we have noticed various cluster sizes as a function of spacer length along with mechanically stronger nanohybrid substrate which again vary in nanohybrids in presence of nanoclay including their biocompatibility which suit them for drug delivery medium. To understand the effect of assembly size, in vitro drug release studies have been performed in phosphate buffer solution ($\text{pH} \approx 7.4$) at 37°C from drug loaded chain extended PUs and their nanohybrids scaffold. The concentration of released drug was measured by using UV-vis absorption studies.^{46–48} Figure 9 shows the cumulative percent ciprofloxacin hydrochloride release as a function of immersion time. The release rate is suppressed drastically with increasing self-assembled

dimension of HHBP-PU against the smaller cluster dimension of BP-PU demonstrating the tunability of drug release by controlling the self-assembled dimension with varying spacer length. In addition, the sustained release of drug from nanohybrids is evident as compared to respective pristine PUs promising fine-tuning of drug release using nanoclay. The dissolution of the drug and its diffusion might be the primary rate determining steps for drug release. The slow release of drug in presence of nanoclays is presumably due to the barrier effect of disk-like nanoparticles for which diffusion of drug molecules gets hindered causing sustained release in nanohybrids. Nonetheless, the dispersed nanoclays in PU matrix are believed to increase the barrier properties by creating a tortuous path that retards the rate of diffusion of drug from the scaffold causing sustained release in nanohybrid and greater self-assembled dimension of PUs for larger chain extenders. However, the drug release can be tuned either by incorporating nanoclays into the matrix or by choosing varying spacer length of chain extender for preparing polyurethanes.

CONCLUSIONS

A new class of polyurethanes has been synthesized using aromatic chain extenders of varying spacer length. Nanohybrids of polyurethanes have been prepared using two-dimensional surface modified nanoclay in situ by dispersing it in poly ol followed by prepolymerization and subsequent chain extension using varying chain extenders. Dramatic and systematic improvement in toughness has been observed for PUs with longer spacer lengths and has been explained using the stronger hydrogen bonding viewpoint occurring for larger spacers in chain extenders. The role of nanoclay in enhancing the mechanical responses of nanohybrids has been explained. Electronic structure calculations have been performed by minimization of energy to predict the intermolecular distance through hydrogen bond. Step-by-step self-assembly has been visualized starting from nanometer level in molecular modeling to micrometer order crystallite observed in optical images through some intermediate stages by small angle neutron scattering (cluster size ~ 20 nm) and band morphology noticed in AFM with dimension ~ 300 nm. In every level, the cluster size enlarges with increasing spacer length which further broadened in nanohybrids in presence of nanoclay. The potential for these novel nanohybrids as biomaterials has well been testified through cell adhesion and cytotoxicity at the gene level. Nanohybrids make conducive environment for cell growth as compared to pristine PU. Finally, the sustained drug delivery has been demonstrated either by controlling the self-assembled pattern by altering the dimension of spacer or by incorporating disk-like nanoclay by making tortuous path rendering delayed diffusion.

ASSOCIATED CONTENT

S Supporting Information. Figures S1–S5 and Tables S1 and S2. This material is available free of charge via the Internet at <http://pubs.acs.org>.

AUTHOR INFORMATION

Corresponding Author

*Tel: 91-542 236 8707; fax: 91-542 236 8707; e-mail: pmaiti.mst@itbhu.ac.in (P.M.).

■ ACKNOWLEDGMENT

The author (A.M.) gratefully acknowledges the financial support from Council for Scientific and Industrial Research (CSIR), New Delhi in the form of fellowship. The authors acknowledge a research grant from the Council for Scientific and Industrial Research (CSIR) Project No. 22(0399)/06/EMR-II). The authors also acknowledge the kind support of Dr. Sudip Malik of IACS, Kolkata, Prof. Gajendra Singh, and Dr. Madhu Yashpal of IMS, BHU for microtomy and TEM observation. The authors acknowledge the kind support of Prof. R.M. Banik for assisting drug release study. Authors are thankful to Dr. D.K. Avasthi and Mr. Pawan K. Kulriya of IUAC, New Delhi for their kind helped during XRD measurements. The authors are also thankful to Prof. S. C. Lakhotia of Department of Zoology, BHU, for Confocal Microscopy, funded by the Department of Science & Technology, India.

■ REFERENCES

- (1) Pochan, D. J.; Chen, Z.; Cui, H.; Hales, K.; Qi, K.; Wooley, K. L. *Science* **2004**, *306*, 94–97.
- (2) Hadjichristidis, N.; Pispas, S.; Floudas, G. A. *Block Copolymer*; Wiley Interscience: New York, 2003.
- (3) Jain, S.; Bates, F. *Science* **2003**, *300*, 460–464.
- (4) Christian, D. A.; Tian, A.; Ellenbroek, W. G.; Levental, I.; Rajagopal, K.; Janmey, P. A.; Liu, A.; Baumgart, T.; Discher, D. E. *Nat. Mater.* **2009**, *8*, 843–849.
- (5) Tomalia, D. A. *Prog. Polym. Sci.* **2005**, *30*, 294–324.
- (6) Bosman, A. W.; Janssen, H. M.; Meijer, E. W. *Chem. Rev.* **1999**, *99*, 1655–1688.
- (7) Gitsov, I.; Lin, C. *Curr. Org. Chem.* **2005**, *9*, 1025–1051.
- (8) Gillies, E. R.; Jonsson, T. B.; Frechet, J. M. J. *J. Am. Chem. Soc.* **2004**, *126*, 11936–11943.
- (9) del Barrio, J.; Oriol, L.; Sanchez, C.; Serrano, J. L.; Cicco, A. D.; Keller, P.; Li, M. H. *J. Am. Chem. Soc.* **2010**, *132*, 3762–3769.
- (10) Riess, G. *Prog. Polym. Sci.* **2003**, *28*, 1107–1170.
- (11) Discher, B. M.; Won, Y. Y.; Ede, D. S.; Lee, J. C.; Bates, F. S.; Discher, D. E.; Hammer, D. A. *Science* **1999**, *284*, 1143–1146.
- (12) Peppas, N. A.; Langer, R. *Science* **1994**, *263*, 1715–1720.
- (13) Lendlein, A.; Langer, R. *Science* **2002**, *296*, 1673–1676.
- (14) Lendlein, A.; Jiang, H. Y.; Junger, O.; Langer, R. *Nature* **2005**, *434*, 879–882.
- (15) Koevoets, R. A.; Versteegen, R. M.; Kooijman, H.; Spek, A. L.; Sijbesma, R. P.; Meijer, E. W. *J. Am. Chem. Soc.* **2005**, *127*, 2999–3003.
- (16) Oertel, G. *Polyurethane Handbook: Chemistry—Raw Materials—Processing—Application—Properties*; Carl Hanser Verlag: Munich, 1993.
- (17) Meckel, W.; Goyert, W.; Wieder, W. *Thermoplastic Elastomers*; Legge, N. R., Holden, G., Schroeder, H. E., Eds.; Hanser Publishers: Munich, 1987.
- (18) Korley, L. T. J.; Liff, S. M.; Kumar, N.; McKinley, G. H.; Hammond, P. T. *Macromolecules* **2006**, *39*, 7030–7036.
- (19) Koerner, H.; Price, G.; Pearce, N. A.; Alexander, M.; Vaia, R. A. *Nat. Mater.* **2004**, *3*, 115–120.
- (20) Liff, S. M.; Kumar, N.; McKinley, G. H. *Nat. Mater.* **2007**, *6*, 76–83.
- (21) Wang, Z.; Pinnavaia, T. J. *Chem. Mater.* **1998**, *10*, 3769–3771.
- (22) Zilg, C.; Thomann, R.; Mulhaupt, R.; Finter, J. *Adv. Mater.* **1999**, *11*, 49–52.
- (23) Xu, R.; Manias, E.; Snyder, A. J.; Runt, J. *Macromolecules* **2001**, *34*, 337–339.
- (24) Mishra, J. K.; Kim, I.; Ha, C. S. *Macromol. Rapid Commun.* **2003**, *24*, 671–675.
- (25) Pattanayak, A.; Jana, S. C. *Polymer* **2005**, *46*, 3275–3288.
- (26) Mishra, A.; Purkayastha, B. P. D.; Roy, J. K.; Aswal, V. K.; Maiti, P. *Macromolecules* **2010**, *43*, 9928–9936.
- (27) Mishra, A.; Aswal, V. K.; Maiti, P. *J. Phys. Chem. B* **2010**, *114*, 5292–5300.
- (28) Winter, M.; Sombroek, D.; Dauth, I.; Moehlenbrink, J.; Scheuermann, K.; Crone, J.; Hofmann, T. G. *Nat. Cell Biol.* **2008**, *10*, 812–824.
- (29) Rinaldo, C.; Prodromo, A.; Siepi, F.; Soddu, S. *Biochem. Cell Biol.* **2007**, *85*, 411–418.
- (30) Gresko, E.; Roscic, A.; Ritterhoff, S.; Vichalkovski, A.; Giannino del, S.; Schmitz, M. L. *EMBO J.* **2006**, *25*, 1883–1894.
- (31) Di Stefano, V.; Rinaldo, C.; Sacchi, A.; Soddu, S.; D’Orazi, G. *Exp. Cell Res.* **2004**, *293*, 311–320.
- (32) Pierantoni, G. M.; Rinaldo, C.; Mottolese, M.; Benedetto, A. D.; Esposito, F.; Soddu, S.; Fusco, A. *J. Clin. Invest.* **2007**, *117*, 693–702.
- (33) Fernandez, C. E.; Bermudez, M.; Munoz-Guerra, S.; Leon, S.; Versteegen, R. M.; Meijer, E. W. *Macromolecules* **2010**, *43*, 4161–4171.
- (34) Klinedinst, D. B.; Yilgor, E.; Yilgor, I.; Beyer, F. L.; Wilkes, G. L. *Polymer* **2005**, *46*, 10191–10201.
- (35) Versteegen, R. M.; Sijbesma, R. P.; Meijer, E. W. *Macromolecules* **2005**, *38*, 3176–3184.
- (36) Versteegen, R. M.; Kleppinger, R.; Sijbesma, R. P.; Meijer, E. W. *Macromolecules* **2006**, *39*, 772–783.
- (37) McLean, R. S.; Sauer, B. B. *Macromolecules* **1997**, *30*, 8314–8317.
- (38) Baumgartner, J. N.; Yang, C. Z.; Cooper, S. L. *Biomaterials* **1997**, *18*, 831–837.
- (39) Hung, H. S.; Wu, C. C.; Chien, S.; Hsu, S. H. *Biomaterials* **2009**, *30*, 1502–1511.
- (40) Reddy, T. T.; Kano, A.; Maruyama, A.; Hadano, M.; Takahara, A. *Biomacromolecules* **2008**, *9*, 1313–1321.
- (41) Wu, Z. Q.; Chen, H.; Huang, H.; Zhao, T.; Liu, X.; Li, D.; Yu, Q. *Macromol. Biosci.* **2009**, *9*, 1165–1168.
- (42) Ding, M.; Li, J.; Fu, X.; Zhou, J.; Tan, H.; Gu, Q.; Fu, Q. *Biomacromolecules* **2009**, *10*, 2857–2865.
- (43) Singh, N. K.; Das Purkayastha, B. P.; Roy, J. K.; Banik, R. M.; Prasad Gonugunta, P.; Misra, M.; Maiti, P. *J. Mater. Chem.* **2011**, *21*, 15919–15927.
- (44) Lahiri, D.; Rouzaud, F.; Namin, S.; Keshri, A. K.; Valdes, J. J.; Kos, L.; Tsoukias, N.; Agarwal, A. *ACS Appl. Mater. Interface* **2009**, *1*, 2470–2476.
- (45) Katti, K. S.; Katti, D. R.; Dash, R. *Biomed. Mater.* **2008**, *3*, 1–12.
- (46) Schierholz, J. M.; Steinhauser, H.; Rump, A. F. E.; Berkels, R.; Pulverer, G. *Biomaterials* **1997**, *18*, 839–844.
- (47) Kwok, C. S.; Horbett, T. A.; Ratner, B. D. *J. Controlled Release* **1999**, *62*, 301–311.
- (48) Depan, D.; Kumar, A. P.; Singh, R. P. *Acta Biomater.* **2009**, *5*, 93–100.